Proceedings of the ASME 2011 30th International Conference on Ocean, Offshore and Arctic Engineering
OMAE2011
June 19-24, 2011, Rotterdam, The Netherlands

OMAE2011-49358

ON LATERAL BUCKLING FAILURE OF ARMOUR WIRES IN FLEXIBLE PIPES

Niels H. Østergaard
NKT-Flexibles /
Aalborg University, Department of Mechanical and Production Engineering
Denmark
Email: Niels.HojenOstergaard@nktflexibles.com

Anders Lyckeggaard
NKT-Flexibles
Jens H. Andreasen
Aalborg University,
Department of Mechanical and Production Engineering

ABSTRACT

This paper introduces the concept of lateral buckling of tensile armour wires in flexible pipes as a failure mode. This phenomenon is governed by large deflections and is therefore highly non-linear. A model for prediction of the wire equilibrium state within the pipe wall based on force equilibrium in curved beams and curvature expressions derived from differential geometry is presented.
On this basis, a model of the global equilibrium state of the armour layers in flexible pipes is proposed. Furthermore, it is demonstrated how this model can be used for lateral buckling prediction. Obtained results are compared with experiments.

INTRODUCTION

Flexible riser pipes are widely used in the offshore industry for oil and gas extraction from subsea reservoirs at water depths so large, that it is not possible or feasible to place a traditional jacket supported oil rig on top of the reservoir. In this case, flexible risers may connect a floating platform to a subsea reservoir. In order to obtain a structural design which provides sufficient structural integrity against external and internal pressures, axial loads and large deflections, flexible pipes are usually designed as unbonded steel-polymer composite structures comprised by a number of layers with different mechanical properties and structural functions. Due to the extreme loading conditions a flexible pipe may experience both during installation and in operation, multiple failure modes have been identified. Most failure modes can today be reconstructed experimentally under controlled conditions and obtained results can be predicted by engineering analysis.
However, a number of failure modes are still subject of academic and industrial research. Among those are lateral buckling of flexible pipe tensile armour layers, which usually are designed as two layers of helically wound steel wires with opposite lay directions. The structural function of the layers is mainly to ensure the integrity of the structure against axial and torsional loads. In order to prevent large radial wire deflections caused by axial compression, which leads to an instability failure mode usually denoted 'birdcaging', see Fig. 1, most risers for deep waters are designed with a high strength tape wound around the wires.
The lateral buckling failure mode has been observed to occur during installation of flexible pipes in ultra deep waters. In the installation scenario, flexible pipes are exposed to axial compression due to hydrostatic pressure on the end cap of an empty pipe, and repeated bending cycles due to vessel movements, waves and current, see Fig. 2. Furthermore, wet annulus conditions (corresponding to a damaged outer sheath) are known to increase the risk of lateral buckling failure, since external pressure does not introduce contact stresses in the wires, which would enable friction to limit wire slippage. The failure mode is governed by very large lateral deflections of the armour wires, see Fig. 3
In order to investigate the physics of the lateral buckling failure mode, it was reproduced experimentally by Braga and Kaleff, [1], in a mechanical test rig. However, it was concluded that failure occured at lower load levels than experienced in the field, and presently this seems like a widely accepted fact. Further experimental studies were conducted and presented by Bectarte and

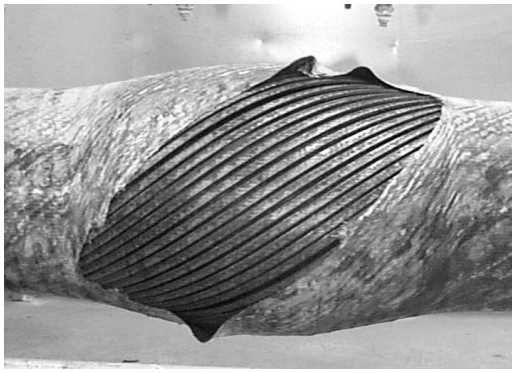

FIGURE 1. Birdcaging failure mode in flexible pipe, generated by NKT-Flexibles by laboratory testing

FIGURE 2. Touch-down zone of flexible pipe during DIP-testing simulating the installation scenario

Coutarel, [2]. Since the results obtained by experiments are not publicly available, a series of experiments are conducted and presented in this paper.

The physical mechanism that leads to lateral buckling failure is presently understood as loss of load carrying capacity of the inner layer of tensile armour wires due to buckling. This causes bending and compression to couple to the pipe torsion, which leads to a severe pipe twist in the pitch direction of the outer layer of amour wires. Due to this twist, the stresses and deformations in the inner layer increases dramatically, which leads to plastic deformation of the layer. Eventually, the pipe structure will therefore be permanently deformed and will in most cases not have the sufficient structural integrity to function in operation.

The mechanics of armour wires have been subject of research for several decades, and numerous examples of research in how to calculate stresses and slips are available. Féret and Bournazel, [3], developed a model for prediction of flexible pipe responses due to axisymmetric loads. Witz and Tan, [4], suggested a model of armour layers in bending, however, assuming the wires to remain in loxodromic configuration (having constant pitch angle). Sævik [6] presented a wire model, in which slip is assumed to occur along a loxodromic curve, for prediction of fatigue lifetime. This research can, however, since transverse slide is neglected, not be used for lateral buckling prediction. Leroy and Estrier, [5], presented research in which transverse wire movements were modeled. However, only force equilibrium in tension and bending was considered. Furthermore, a prescribed experience based solution-form was chosen, which cannot be expected to hold in compression. Brack et. al. [7] demonstrated that the non-linear buckling load of an armour wire could be calculated by a finite-element model. However, in order to study the coupling effects leading to failure of an armour layer, an analytical model taken transverse equilibrium into account needs to be developed.

FIGURE 3. Lateral buckling in the inner layer of tensile armour wires, generated by NKT-Flexibles by laboratory testing

The presented research aims to determine the limit state of the tensile armour wires after many bending cycles have been applied. It is noted, that while this approach is reasonable when modeling wire buckling, it is just one of many approaches to wire mechanics, and other approaches may provide better results with respect to other failure modes.

1 METHODS

1.1 Single wire mechanics

The geometry, equilibrium and constitutive relations for a single tensile armour wire subjected to axial loads and bending will be considered in this section. The radius of curvature will, for the sake of simplicity, be assumed constant. A single armour wire can therefore be considered as constituting a curve on a torus surface.

Friction will, in order to determine the limit equilibrium state of a wire subjected to given loads, be neglected. Slip towards this limit state will occur, since the pipe annulus is considered flooded, so friction does not restrain the wires to a loxodromic

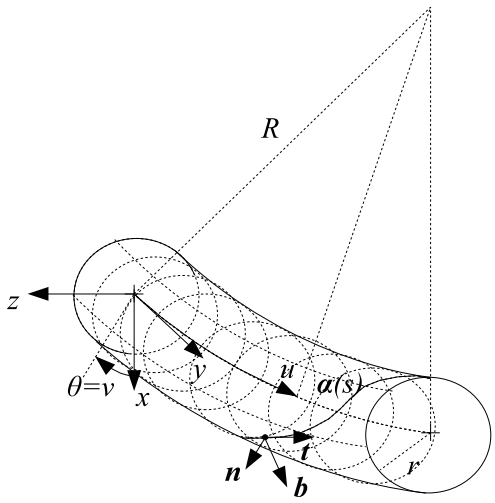

FIGURE 4. Wire geometry

configuration.

While the curvature components of a single tensile armour wire in the analysis are allowed to be large, the axial strain of the wire is assumed sufficiently small to determine using Cauchy's definition of strain. It will furthermore be assumed that the curvature components can be determined on basis of the geometry of an inextensible curve due to small axial strains.

A parameterization of the torus by an arc length coordinate u along the torus centerline and an angular coordinate v is chosen, see figure 4. The torus surface is then, for pipe curvature $\kappa = \frac{1}{R}$ and radius r given by

$$\mathbf{x}(u,v) = \begin{bmatrix} \left(\frac{1}{\kappa} + r\cdot\cos v\right)\cos(\kappa u) - \frac{1}{\kappa} \\ \left(\frac{1}{\kappa} + r\cdot\cos v\right)\sin(\kappa u) \\ r\cdot\sin v \end{bmatrix} \tag{1}$$

A curve α can be constructed by relating u and v. Assuming the curve parameterized by undeformed arc length s_0, a curvilinear coordinate triad of unit length given by

$$\mathbf{t} = \frac{d\alpha}{ds_0} \qquad \mathbf{n} = \frac{\mathbf{x}_u \times \mathbf{x}_v}{\|\mathbf{x}_u \times \mathbf{x}_v\|} \qquad \mathbf{b} = \mathbf{t} \times \mathbf{n} \tag{2}$$

can be attached to each point on the curve. Now considering the geometry of the wire in the tangent plane, an alternative definition of the unit tangent vector is as a linear combination of the following two unit vectors spanning the tangent plane of the torus surface

$$\mathbf{t}_u = \frac{\mathbf{x}_u}{\|\mathbf{x}_u\|} \quad \mathbf{t}_v = \frac{\mathbf{x}_v}{\|\mathbf{x}_v\|} \tag{3}$$

in which the surface derivatives are given by

$$\mathbf{x}_u = \frac{\partial \mathbf{x}}{\partial u} \quad \mathbf{x}_v = \frac{\partial \mathbf{x}}{\partial v} \tag{4}$$

With the definitions given in equation 3 and 4, a wire tangent vector can be defined as

$$\mathbf{t} = \cos\phi\,\mathbf{t}_u + \sin\phi\,\mathbf{t}_v \tag{5}$$

in which ϕ denotes the wire angle with respect to $\mathbf{t}_u$. In order for this definition to be consistent with the definition given in equation 2, the following vectorial equation must hold

$$\begin{aligned} \frac{d\alpha}{ds_0} &= \mathbf{x}_u\frac{du}{ds_0} + \mathbf{x}_v\frac{dv}{ds_0} \\ &= \cos\phi\,\mathbf{t}_u + \sin\phi\,\mathbf{t}_v \end{aligned} \tag{6}$$

This corresponds to stating

$$\frac{du}{ds_0} = \frac{\cos\phi}{\|\mathbf{x}_u\|} \qquad \frac{dv}{ds_0} = \frac{\sin\phi}{\|\mathbf{x}_v\|} \tag{7}$$

Equation 11 relates the arc length derivatives to the wire angle and surface geometry. The effect of that the arc length s in the loaded wire state does not correspond to the arc length in the initial helical state s_0 will now be taken into calculation by modification of the tangent length. Considering the initial wire geometry parameterized by undeformed arc length s_0, the axial wire strain ε can be related to s by

$$ds = (1+\varepsilon)ds_0 \tag{8}$$

The length of the tangent vector for a curve parameterized by s is given by

$$\mathbf{t}\cdot\mathbf{t} = (1+\varepsilon)^2 \tag{9}$$

The following definition of the tangent vector fulfills this requirement

$$\mathbf{t} = (1+\varepsilon)\cos\phi\,\mathbf{t}_u + (1+\varepsilon)\sin\phi\,\mathbf{t}_v \tag{10}$$

This corresponds to stating

$$\frac{du}{ds} = (1+\varepsilon)\frac{\cos\phi}{\|\mathbf{x}_u\|} \qquad \frac{dv}{ds} = (1+\varepsilon)\frac{\sin\phi}{\|\mathbf{x}_v\|} \tag{11}$$

Calculating $\mathbf{x}_u$ and $\mathbf{x}_v$ as defined in equation 4, the following norms can be determined

$$\|\mathbf{x}_u\| = 1 + r\kappa\cos v \qquad \|\mathbf{x}_v\| = r \tag{12}$$

Since the governing equations for the wire tangent geometry have now been derived, curvature components of the wire must be calculated. Applying the well-known Darboux frame, the triad vectors and their first order derivatives in arc length can be related by the curvature components

$$\frac{d}{ds_0}\begin{bmatrix}\mathbf{t}\\ \mathbf{n}\\ \mathbf{b}\end{bmatrix} = \begin{bmatrix}0 & \kappa_n & -\kappa_g\\ -\kappa_n & 0 & \tau\\ \kappa_g & -\tau & 0\end{bmatrix}\begin{bmatrix}\mathbf{t}\\ \mathbf{n}\\ \mathbf{b}\end{bmatrix} \tag{13}$$

The chosen sign convention can be shown to correspond to, that a positive rotation about a given axis corresponds to a positive change of curvature for a positive change of arc length, and is furthermore consistent with respect to the sign conventions chosen in [5] and [6]. Furthermore, this choice of sign convention secures that moments and changes of curvature have the same sign, which is desirable when formulating constitutive relations, see equation 25. Applying this definition to a coordinate frame defined as specified in equation 2, the following wire curvature components can be derived

$$\kappa_n = -\frac{\kappa\cos v}{1+r\kappa\cos v}\cos^2\phi - \frac{1}{r}\sin^2\phi \tag{14}$$

$$\kappa_g = \left(\frac{\kappa\sin v}{1+r\kappa\cos v}\cos\phi + \frac{d\phi}{ds}\right) \tag{15}$$

$$\tau = \left(\frac{\kappa\cos v}{1+r\kappa\cos v} - \frac{1}{r}\right)\cos\phi\sin\phi \tag{16}$$

The obtained curvature components can be compared with components derived by Leroy and Estrier, [5], chosing a loxodromic curve on a torus surface as reference curve, see Fig. 5. The curvature components can be observed to be of the same magnitude and differences in signs can be observed to correspond to different sign conventions. Since the wire geometry has now been considered, a set of equilibrium equations must be derived. The equilibrium equations of a curved beam are given by Reissner, [8], on vectorial form

$$\frac{d\mathbf{P}}{ds} + \mathbf{p} = 0 \qquad \frac{d\mathbf{M}}{ds} + \mathbf{t}\times\mathbf{P} + \mathbf{m} = 0 \tag{17}$$

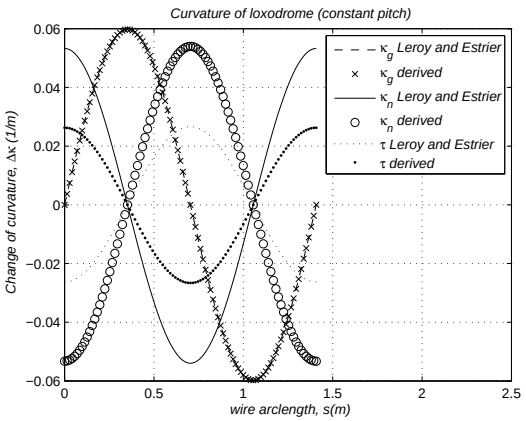

FIGURE 5. Curvature components of loxodromic curve

The internal and external force and moment-vectors in equations 17 are given by

$$\begin{aligned}\mathbf{P} &= P_t\mathbf{t} + P_n\mathbf{n} + P_b\mathbf{b}\\ \mathbf{M} &= M_t\mathbf{t} + M_n\mathbf{n} + M_b\mathbf{b}\\ \mathbf{p} &= p_t\mathbf{t} + p_n\mathbf{n} + p_b\mathbf{b}\\ \mathbf{m} &= m_t\mathbf{t} + m_n\mathbf{n} + m_b\mathbf{b}\end{aligned} \tag{18}$$

Applying equation 13, the equilibrium equations can be rewritten on component form

$$\frac{dP_t}{ds} - \kappa_n P_n + \kappa_g P_b + p_t = 0 \tag{19}$$

$$\frac{dP_n}{ds} + \kappa_n P_t - \tau P_b + p_n = 0 \tag{20}$$

$$\frac{dP_b}{ds} - \kappa_g P_t + \tau P_n + p_b = 0 \tag{21}$$

$$\frac{dM_t}{ds} - \kappa_n M_n + \kappa_g M_b + m_t = 0 \tag{22}$$

$$\frac{dM_n}{ds} + \kappa_n M_t - \tau M_b - P_b + m_n = 0 \tag{23}$$

$$\frac{dM_b}{ds} - \kappa_g M_t + \tau M_n + P_n + m_b = 0 \tag{24}$$

Since the surface is considered frictionless, the external forces p_b and p_t in the tangent plane and the distributed moments m_b and m_n can be considered zero.
Assuming the wire dimensions small both with respect to major and minor torus radii, it is fair to neglect curved beam terms in the cross sectional constants and assume the wire constitutive

equations linear. These are given by

$$\begin{aligned} P_t &= EA\varepsilon \\ M_t &= GJ\Delta\tau \\ M_b &= EI_b\Delta\kappa_n \\ M_n &= EI_n\Delta\kappa_g \end{aligned} \tag{25}$$

Now considering the equations governing the tangent wire geometry in equation 11, rearranging the obtained definition of the geodesic curvature and considering equilibrium in the tangent plane, the following consistent sixth order system is obtained

$$\frac{du}{ds} = (1+\varepsilon)\frac{\cos\phi}{1+r\kappa\cos v} \tag{26}$$
$$\frac{dv}{ds} = (1+\varepsilon)\frac{\sin\phi}{r} \tag{27}$$
$$\frac{d\phi}{ds} = -\frac{\kappa\sin v}{1-r\kappa\cos v}\cos\phi + \kappa_g \tag{28}$$
$$\frac{dP_t}{ds} = \kappa_n P_n - \kappa_g P_b \tag{29}$$
$$\frac{dP_b}{ds} = \kappa_g P_t - \tau P_n \tag{30}$$
$$\frac{dM_n}{ds} = -\kappa_n M_t + \tau M_b + P_b \tag{31}$$

in which remaining unknown functions are given in terms of known quantities after a solution is found. The system can be solved with respect to boundary conditions corresponding to the mechanical behavior of flexible pipe end fittings, in which the wires are fixed in displacement and rotation

$$u(0) = 0 \quad v(0) = v^A_{ini} \quad \phi(0) = \phi_{hel} \tag{32}$$

$$u(S) = L\left(1+\frac{\Delta L}{L}\right) \quad v(S) = v^B_{ini} - \frac{\Delta\psi}{L}L \quad \phi(S) = \phi_{hel} \tag{33}$$

in which S denotes the total wire arc length, ϕ_{hel} the initial helical wire lay angle and v^A_{ini} and v^B_{ini} the specified v-coordinate of the wire, respectively, for $s = 0$ and $s = S$. Furthermore, $\frac{\Delta L}{L}$ denotes the pipe strain and $\frac{\Delta\psi}{L}$ the pipe twist, which correspond to the applied generalized loads.

A system of equations for prediction of the wire equilibrium state has now been derived allowing for large transverse slips.

Modeling an armour wire with the conventional assumption, that the wire angle remains constant such that the wire constitutes a loxodromic curve on a torus surface, the derived system can be simplified. Setting $\frac{d\phi}{ds} = 0$ corresponding to constant pitch angle, the expression for the geodesic curvature reduces to

$$\kappa_g = \frac{\kappa\sin v}{1+r\kappa\cos v}\cos\phi \tag{34}$$

With $\frac{d\phi}{ds} = 0$ all curvature components are only functions of v and ϕ. Relating changes of curvature with sectional wire moments by applying the constitutive equations, the binormal sectional wire force is now determined by the normal moment equilibrium. The governing equations can then be reduced to

$$\frac{du}{ds} = (1+\varepsilon)\frac{\cos\phi}{1+r\kappa\cos v} \tag{35}$$
$$\frac{dv}{ds} = (1+\varepsilon)\frac{\sin\phi}{r} \tag{36}$$
$$\frac{d\phi}{ds} = 0 \tag{37}$$
$$\frac{dP_t}{ds} = \kappa_n P_n - \kappa_g P_b \tag{38}$$

The corresponding boundary conditions are

$$u(0) = 0 \quad v(0) = v^A_{ini} \tag{39}$$

$$u(S) = L\left(1+\frac{\Delta L}{L}\right) \quad v(S) = v^B_{ini} - \frac{\Delta\psi}{L} \tag{40}$$

The solutions to the presented boundary value problems are in the following determined using a Matlab build-in solver by the Lobatto-IIIa method.

It is noted, that since the wire is considered embedded in a torus surface, the rotation around the wire tangent is governed only by the underlying surface. In a physical pipe structure, the wire may under some circumstances to some extend be allowed to rotate in a slightly different manner causing a phenomenon which is usually denoted 'fishscaling'. This leads to a model which has a larger stiffness than the wire being modeled. The effect is, however, due to contact effects from adjacent layers and in accordance with observations made during conducted experiments deemed negligible in the present context.

1.2 Flexible pipe model

A model for prediction of the flexible pipe torsional response to compression and bending can now, if transverse wire contact is neglected, be constructed on basis of multiple single wire analyses. The global torsional boundary conditions of the analyzed

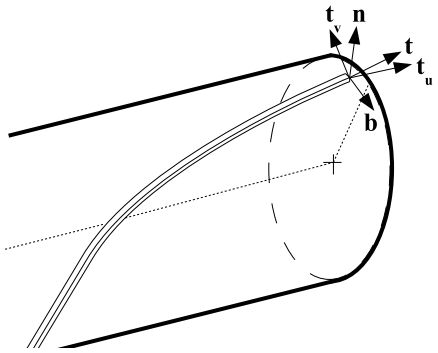

FIGURE 6. Wire coordinate triads

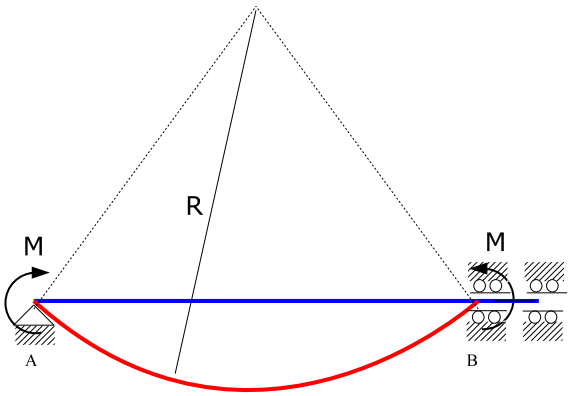

FIGURE 7. Flexible pipe model

pipe will be taken as fixed-free corresponding to the conducted lateral buckling laboratory experiments, see Fig. 7.
While the inner layer of tensile armour will be considered free to seek equilibrium transversely, the outer layer will be assumed locked in loxodromic configuration. The underlying assumption, that no transverse slip occurs in the outer layer of armour wires, is supported by observations made during execution of experiments, by which no transverse slip or change of lay angles could be observed in the outer layer of armour wires, even when severe failure was detected in the inner layer of tensile armour.

In order for the free end of the flexible pipe to be in equilibrium, a pipe twist $\frac{\Delta\psi}{L}$ must be applied such that the following global equation of equilibrium is satisfied

$$\sum_{i=1}^{n_{wires}} (M_u^i - P_v^i \cdot r^i) + \sum_{i=1}^{n_{sheets}} M_{u,sheets}^i = \quad (41)$$

$$\sum_{i=1}^{n_{wires}} \left(M_t^i cos\phi^i + M_b^i sin\phi^i - (P_t^i sin\phi^i - P_b^i cos\phi^i) \cdot r^i\right) + \sum_{i=1}^{n_{sheets}} G^i J^i \frac{\Delta\psi}{L} = 0$$

in which forces P and moments M are calculated with respect to the u and v-directions given on Fig. 6. Once the geometrical configuration satisfying equation 41 has been established, the axial loads carried by the pipe structure can be calculated as

$$\begin{aligned} P_a &= \sum_{i=1}^{n_{wires}} P_u^i + \sum_{i=1}^{n_{sheets}} P_{u,sheets}^i \quad (42) \\ &= \sum_{i=1}^{n_{wires}} P_t^i cos\phi^i + P_b^i sin\phi^i + \sum_{i=1}^{n_{sheets}} E^i A^i \frac{\Delta L}{L} \end{aligned}$$

Torsional equilibrium can be establish by solving equation 41 for given generalized load inputs, pipe bending radius R and axial pipe strain $\frac{\Delta L}{L}$ by Newton-Raphton iterations.
The presented model does not take radial deformations due to axisymmetric loadings into calculation. It will, in order to study the effect of a radially elastic pipe wall be assumed, that the radial expansion in the model equals the radial expansion obtained by axisymmetric analysis be means described in [3]. While this assumption can be justified for loadings which do not cause the inner layer of tensile armour to fail by lateral buckling, it does not provide sufficient precision after failure has occurred. The main reason for this is, that the applied methods are based on axisymmetric loading of perfect helices, and the wire geometry may change dramatically as the wires buckle. From axisymmetric analysis it is known that

$$P_a = k_a \frac{\Delta L}{L} = -k_r \frac{\Delta r}{r} \quad (43)$$

in which k_a and k_r denotes the axial and radial stiffness of a flexible pipe modeled with linear global properties. Defining the radial strain and rearranging equation 43 yields

$$r_d = \left(1 + \frac{\Delta r}{r}\right) r = \left(1 - \frac{k_a}{k_r} \frac{\Delta L}{L}\right) r \quad (44)$$

The radius in the torus model can therefore be considered a function of the applied axial loading, while initial curvature components are calculated on basis of the radius in the unloaded state. Since the system of governing equations for the wires in the inner layer is non-linear, an imperfection must be added to the geometry, in order to trigger stability phenomena if present. The

TABLE 1. 6” FLEXIBLE PIPE DESIGN

-	Inner layer	Outer layer
$OD(m)$	0.2012	0.209
$L_{pitch}(m)$	1.263	1.318
Wire size (mm)	3×10	3×10
Number of wires	52	54

imperfection can be added directly to the geodesic curvature as

$$\kappa_{g,pert} = \kappa_g + \sum_{i=1}^{m} \gamma_i sin\left(\frac{i\pi s}{L}\right) \tag{45}$$

with $m = 20$ and $\gamma_{amp} = -0.001$.

2 RESULTS

A 6” flexible pipe with tensile armour properties given in table 1 will be modeled. Effects from other pipe layers are neglected. It is noted, that polymer sheaths, insulation and high-strength tape layers of flexible pipes may in some cases contribute significantly to the torsional- and compressive pipe stiffness. However, for the present pipe design, this is not the case. The wires are made of steel with elastic modulus $2.1 \cdot 10^5 MPa$, yield stress $765MPa$ and are considered isotropic. In order to study the structural behavior in compression, the (load-strain)-curve of the loaded end of the pipe will be presented for various model parameters, see Fig. 8. Two different bending radii will be studied for radially stiff pipe structures. Furthermore, a radially elastic pipe structure will be analyzed by applying equation 44. All responses exhibit significant softening behavior, which is interpreted as limit point buckling. Considering the obtained equilibrium state of the wires, the added imperfection can be observed to cause wire gaps to localize in one end of the analyzed pipe, see Fig. 9. Both the pipe curvature and the effect of radial expansion can be observed to have very limited influence on the buckling load in the analyzed flexible pipe. However, the approach by which radial expansion is taken into calculation, can for obvious reasons not be considered exact and can therefore only be considered as an estimate.

Considering the twist angle of the free end of the flexible pipe, this can be observed also exhibit limit point behavior, see Fig. 10. The physical interpretation of this result is, that when the pipe is subjected to loads equal to or larger than the limit point buckling load, it will cause a severe twist. Calculating the stresses in all wires in the equilibrium state, the maximum stress in the armour layers can be determined, see Fig. 11.

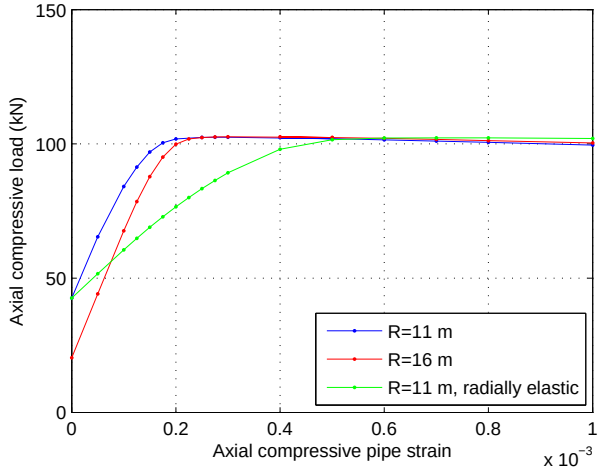

FIGURE 8. (Load-strain)-curve for different bending radii, R

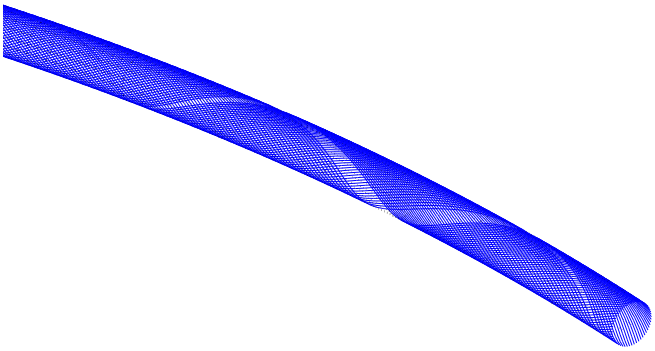

FIGURE 9. Localized wire buckling

3 MODEL-EXPERIMENT COMPARISON

In order to reconstruct the lateral buckling failure mode in the laboratory, experiments were carried out on three 5 meter long 6” pipe samples with armour layer design given in Tab. 1 in mechanical test rigs, see Fig. 12. The test setup was quite similar to the one applied by Braga and Kaleff, [1]. The pipe samples were mounted with geometrical boundary conditions corresponding to the ones shown in Fig. 7. Compression was applied by mounting a smaller flexible pipe inside the test pipe. Subjecting this to tension caused a compressive reaction in the test sample. Cyclic bending from neutral position to a specific maximum pipe curvature was applied by rotating the pinned frames on which the pipe endfittings were mounted. In one case, a large number of bending cycles were applied without sign of failure in the test sample. After the initial test cycle had been concluded, the test pipe was tensioned in cyclic bending in order

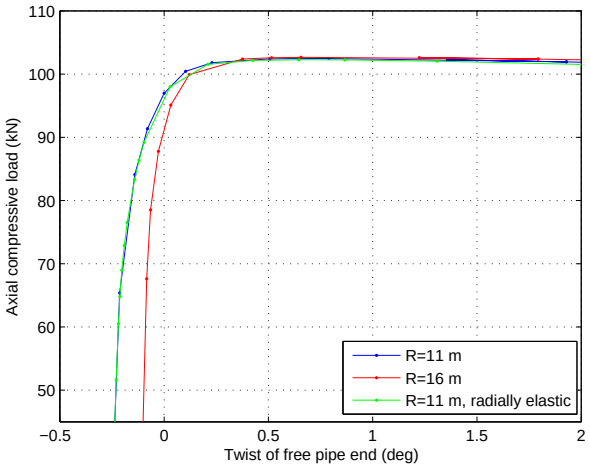

FIGURE 10. Pipe twist for different bending radii, *R*

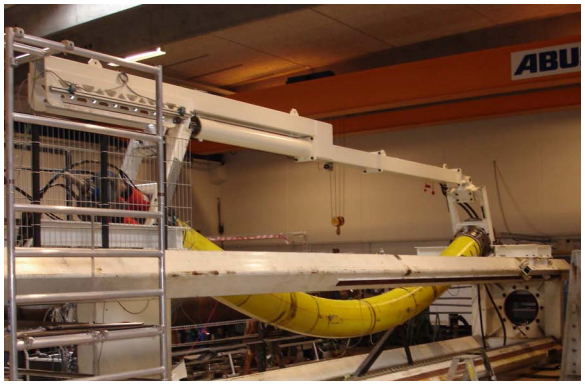

FIGURE 12. Lateral buckling test rig

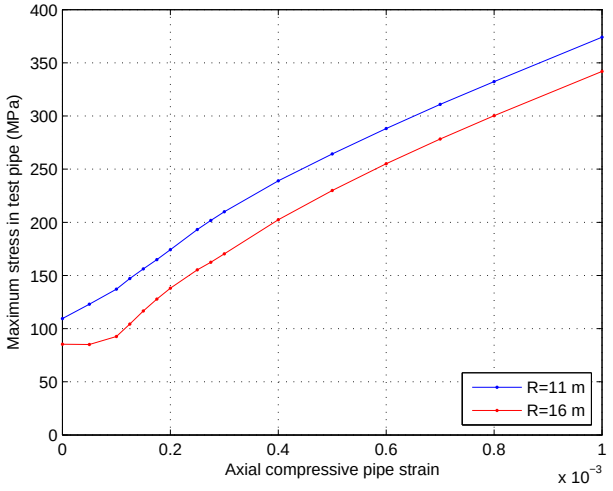

FIGURE 11. Maximum wire stress

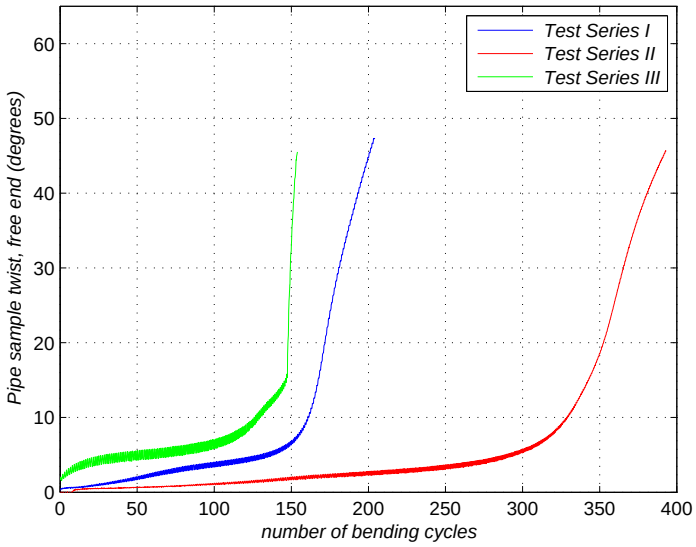

FIGURE 13. Twist responses measured during laboratory testing

to straighten the wires within the pipe wall, and the test pipe was finally subjected to compressive loads larger than during the initial test cycle. This caused failure by lateral buckling in the test pipe.

The key difference between results obtained from the model and experiments is, that while modeled wires fail immediately when critical loads are applied, cyclic bending must be applied in the experiments to overcome frictional effects before failure occurs. The measured twist of the free end of the test sample is presented in Fig. 13. It is during laboratory testing observed, that the pipe curvature has large influence on the number of bending cycles which must be applied in order to trigger failure by lateral buckling.

In Fig. 14 buckling mode shapes determined experimentally and by modeling are compared. Buckling mode A. corresponds to large wire gaps, while buckling mode B. corresponds to a geometrical state with large deviations from the initial helical angle but with small gaps. It is noted, that while gaps in mode A. localize similar in test and model results, mode B. is detected as localized buckling during experiments, but as a periodic solution throughout the pipe length in the model. However, this mode has in the current case occurred in the model after the yield strength has been exceeded in the wires. This may explain the difference

A.

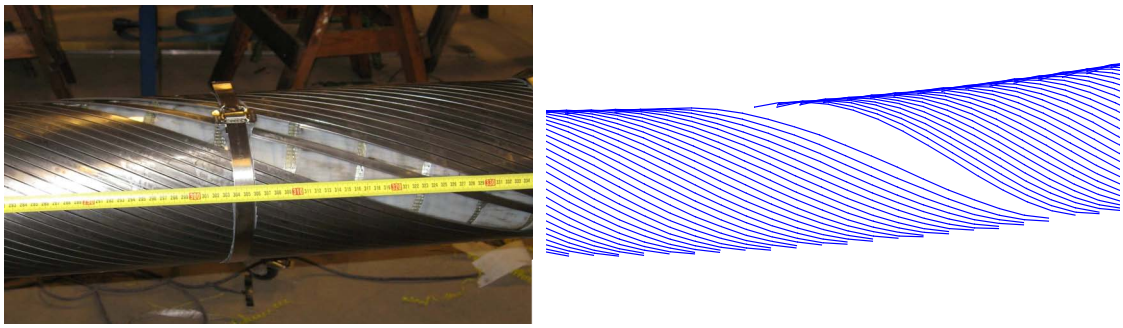

B.

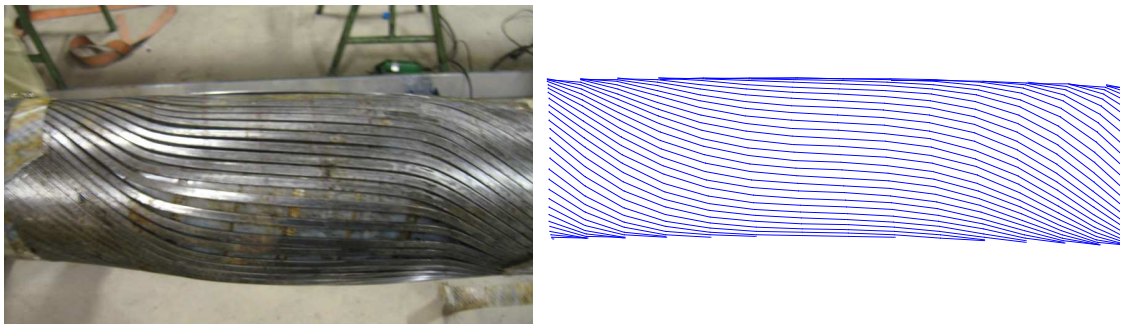

FIGURE 14. Detected buckling modes

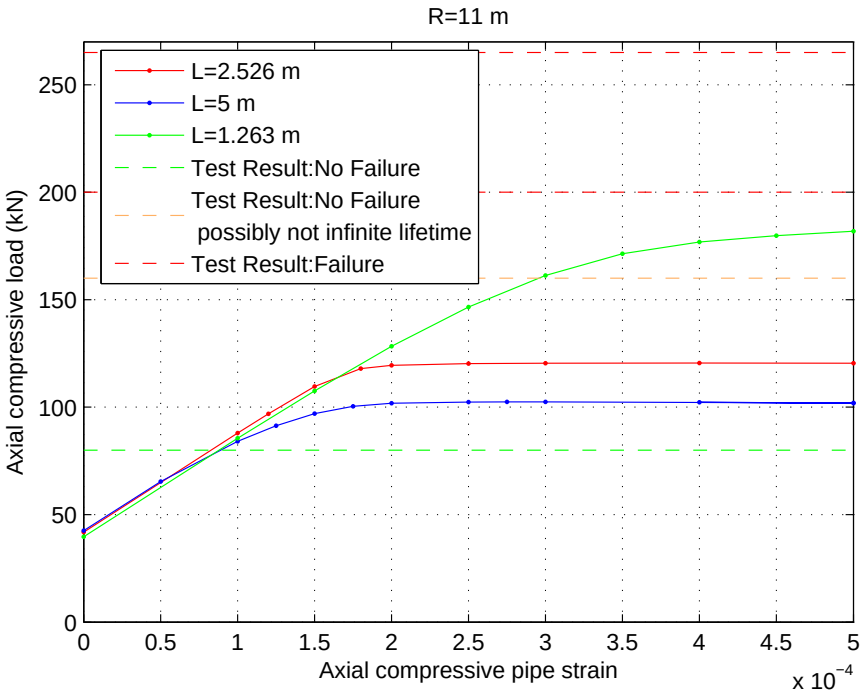

FIGURE 15. Model-experiments comparison

between results. In Fig. 15 the calculated axial load carried by the pipe structure is compared to tests results for a fixed bending radius of $11m$. Two test results can be observed to be, that lateral buckling was not triggered in the test pipe, in which infinite lifetime may not be guaranteed in one case. Furthermore, two tests can be observed to have failed by lateral buckling. These are represented by the two red dotted lines in the figure. If the model length is set equal to the physical length of the test sample, the model can be observed to generate a conservative estimate for the limit load. However, it is a well-known fact that end-fitting effects on the wires combined with friction causes the wires in zones close to end-fittings to be restrained in their positions during bending. The effect of non-slip zones can be estimated by setting the model length shorter than the physical length of the pipe sample, since both slip-free zones in each end of the pipe sample will deform rigidly. Assuming that only respectively one and two pitches are free to slide, the buckling load can be calculated. While decreasing the model length to two pitches can be observed to have moderate influence on the buckling load, the model of one pitch length exhibits a dramatically larger buckling load than the original model. A model length this short cannot be justified on physical grounds on basis of the research presented in this paper, but is included in the comparison in order to demonstrate that the difference between the two models with modified length is significant. The physical reason for this is, that if less than two pitches are free to slip transversely, the obtained buckling mode is influenced severely, so a different mode shape is determined.

4 CONCLUSIONS

In order to develop a method, which can predict lateral buckling of the tensile armour wires in flexible pipes, theoretical and experimental studies have been conducted.

A mathematical single wire model based on equilibrium of curved beams and curvature expressions derived on basis of differential geometry has been presented. Since the wire is assumed to rest on a frictionless surface, the equilibrium state of the wire is reached immediately when loads are applied, while cyclic loadings must be applied to a physical pipe structure in order to overcome frictional effects so the equilibrium state is reached.

On basis of the single wire model, a mathematical model of an entire flexible pipe can be obtained by multiple single wire analyses, if transverse contact between the wires is neglected. This model can be used to determine the torsional equilibrium state for a flexible pipe subjected to given compressive and bending loads.

This model exhibits behavior quite similar to the observations made during experiments and can be applied in order to obtain a conservative estimate of the limit buckling load, which can be carried by the pipe structure. However, since friction is not included in the model, only the limit load for which lateral buckling will never occur can be determined.

The friction may along with end-fitting effects cause, that the wires in each end of the analyzed pipe will never experience slip, since they are locked in their positions. The impact of this effect on the results can be estimated by setting the length of the mathematical model lower than the physical length of the test pipe. Results show that this effect may impose severe impact on the buckling load.

Future research will therefore include a method for determination of the length of the slip-free zones in each end of the test sample. Furthermore, additional experiments will be conducted in order to validate the obtained model.

REFERENCES

[1] Braga, M.P. and Kaleff, P. (2004): Flexible Pipe Sensitivity to Birdcaging and Armor Wire Lateral Buckling. Proceedings of OMAE, 2004

[2] Bectarte,F. and Coutarel,A. *(2004): Instability of Tensile Armour Layers of Flexible Pipes under External Pressure.* Proceedings of OMAE, 2004

[3] Féret, J.J. and Bournazel, C.L. (1987): Calculation of stresses and slips in structural layers of unbonded flexible pipes. Journal of Offshore Mechanics and Arctic Engineering, Vol. 109

[4] Witz, J.A. and Tan, Z. (1992): On the Flexural Structural Behaviour of Flexible Pipes, Umbillicals and Marine Cables. Marine Structures, Vol. 5

[5] Leroy, J.M. and Estrier, P. (2001): Calculation of stresses and slips in helical layers of dynamically bent flexible pipes. Oil and Gas Science and Technology, REV. IFP, Vol. 56, No. 6, pp. 545-554, 2001

[6] Sævik, S. (1993): A finite element model for predicting stresses and slip in flexible pipe armouring tendons. Computers and Structures. Vol. 46, No.2

[7] Brack. A., Troina, L.M.B. and Sousa, J.R.M. (2005): Flexible Riser Resistance Against Combined Axial Compression, Bending and Torsion in Ultra-Deep Water Depths. Proceedings of OMAE, 2005

[8] Reissner, E. (1981): On finite deformations of space-curved beams. Journal of Applied Mathematics and Physics (ZAMP), Vol. 32